

Development of Sloped Rolling-Type Isolation Devices for Seismic Protection of Important Equipment and Facilities

S.J. Wang, C.H. Yu & J.Y. Hsiao

National Center for Research on Earthquake Engineering, Taipei, Taiwan

J.S. Hwang

National Taiwan University of Science and Technology, Taipei, Taiwan

K.C. Chang & M.S. Tsai

National Taiwan University, Taipei, Taiwan



SUMMARY:

To seismically protect critical equipment or facilities inside an existing building without employing any modern structural control technologies, the implementation of seismic isolation technologies to the equipment or facilities may be one of the most practical and effective methods. In this study, the dynamic behavior and design requirements of the sloped rolling-type isolation devices with multi-roller and inbuilt damping mechanisms are thoroughly investigated. In addition to having a good potential to control the transmitted acceleration response as a steady level, the multi-roller mechanism has better stability performance and re-centering capability than the conventional single-roller mechanism. Moreover, the inbuilt damping mechanism facilitates to suppress excessive displacement responses and to stop rolling motion after earthquakes. Based on the analytical results, a simplified mathematical hysteretic model is proposed to represent the twin-flag hysteresis loop of the isolation device. The shaking table test results on several plane arrangements of isolated reservation cabinets and an isolated raised floor system show that the adoption of the isolation devices are effective in reducing seismic demands for the protected objects.

Keywords: rolling-type isolation device, multi-roller, inbuilt damping mechanism, simplified hysteretic model, shaking table test

1. INTRODUCTION

The performance-based design for building structures is recently attracting immense attention in the earthquake engineering community. It is especially emphasized that the seismic performance of some specific buildings depends on not only the seismic-resistant capabilities of their structural components but also the functionality of their contents. That is, even structural elements can remain intact during or after earthquakes, the desired performance of the buildings may not be achieved due to malfunction or even damage of the housed vibration-sensitive equipment or facilities. This phenomenon has occurred commonly during or after many historical earthquakes. For instance, (1) computers, servers, data storage equipment, networks and telecommunications in high-tech industries, telecom industries, banks, emergency-response centers and data centers cannot remain operational; (2) high-precision equipment, power generators and medical instruments in high-tech factories and hospitals cannot remain functional; and (3) valuable antiques and exhibits in museums suffered serious damage. The past lessons have caused awareness of enhancement of seismic performance for the critical equipment and facilities in the relevant industries and organizations (Hwang *et al.*, 2004; Myslimaj *et al.*, 2003).

In order to mitigate seismic risks posed to vibration-sensitive equipment or facilities inside an existing building without employing any modern structural control technologies, the implementation of seismic isolation technologies, instead of conventional restraints, to the equipment or facilities may be one of the most practical and effective methods. The currently available passive isolation bearings can be classified into four primary types: (1) elastic; (2) elastomeric (Naeim *et al.*, 1999); (3) sliding-based (Hamidi *et al.*, 2003); and (4) rolling-based (Lin *et al.*, 1993; Zhou *et al.*, 1998; Tsai *et al.*, 2007; Lee *et al.*, 2010). Sufficient horizontal flexibility and efficient re-centering capability after earthquakes are

essential features for all these isolation bearings. Besides, inbuilt or additional energy dissipation capabilities are in general required for a better seismic performance control. Considering less dependence on the protected object weight and limited impacts on the existing working conditions, sliding-based and rolling-based metal isolation bearings with adequate energy dissipation mechanisms are more commonly used to prevent the vibration-sensitive equipment or facilities from malfunction or damage due to excessive acceleration responses during earthquakes. If a whole region at which the equipment vulnerable to earthquakes is located needs to be protected, it is more systematic and more economical to incorporate seismic isolation bearings into to a raised floor system, i.e. the isolated raised floor system, which is also valid for new constructed structures. Many studies also revealed that for a better displacement control of passive isolation bearings especially while subjected to excitations with strong long-period components, active or semi-active control devices with an adaptive feature were suggested to be incorporated into the isolation system, which is generally named as “smart” or “hybrid” isolation system (Lu *et al.*, 2008). Although these smart or hybrid systems may have a better seismic performance compared to purely passive systems, the requirements of additional sensors and actuators with feedback control loops may make them more complex than purely passive systems.

Among the aforementioned isolation devices for seismic protection of equipment or facilities, the rolling-based isolation device employing rolling motion of cylindrical rollers between two opposite bearing plates with a constant sloping surface is capable of transmitting a steady acceleration response to the protected object no matter what excitations are undergone. Four important features for such an isolation device are addressed as follows: (1) the isolation device can offer maximum horizontal decoupling between the protected object and input excitations since it does not have a fixed vibration natural period; (2) the horizontal seismic force transmitted to the protected object can be reduced significantly since the rolling friction force and the restoring force due to gravity of the isolation device are much smaller than the input horizontal seismic force; (3) the horizontal peak transmitted acceleration response can remain as a steady level regardless of any input motion, which can meet the rigorous performance-based design requirements for the protected object; and (4) the isolation device has an efficient inherent gravity-based self-centering capability after earthquakes. These features aforementioned make the device have a good potential to be applied to passive, semi-active and active seismic isolation systems. Therefore, the dynamic behavior of the sloped rolling-type isolation device equipped with two pairs of mutually orthogonal rollers, i.e. the multi-roller isolation device, adopting different design parameters, such as sloping angles and supplemental damping mechanisms, are analytically investigated in this study. To verify the analytical results, several plane arrangements of isolated reservation cabinets and an isolated raised floor system subjected to recorded strong ground motions and artificial acceleration histories are performed in the shaking table test schemes.

2. MECHANICAL FEATURES AND DYNAMIC BEHAVIOR OF MULTI-ROLLER ISOLATION DEVICES

2.1. Derivation of Equations of Motion

The multi-roller isolation device is typically composed of three bearing plates (denoted as upper, intermediate and lower bearing plates) and two pairs of mutually orthogonal cylindrical rollers, as schematically shown in Figure 1. Along each of two orthogonal directions, a pair of rollers is sandwiched between two opposite bearing plates in which both or one have dual V-shaped sloping surfaces. The rolling motions of two pairs of mutually orthogonal rollers make feasible in-plane seismic isolation functionality. The multi-roller mechanism makes possible synchronous movement for the rollers in each principle horizontal direction and can effectively prevent sliding motions between rollers and bearing plates. Therefore, it has better stability performance and self-centering capability compared to the conventional single-roller mechanism. It is noted that to prevent undesired instant collision when the roller passes through the valley of the V-shaped surface, an arched range with a fixed curvature radius which is much larger than the roller radius is proposed to be reserved between two inclines of the V-shaped surface of the bearing plate. Besides, due to the limited energy dissipation capability contributed by rolling friction, additional sliding friction dampers are suggested

to be appropriately inbuilt in the isolation device. Learning from the previous studies (Tsai *et al.*, 2007; Lee *et al.*, 2010), this paper first aims to thoroughly investigate the dynamic behavior of the multi-roller isolation devices adopting the following different design parameters: (1) rollers move between two V-shaped sloping surfaces (i.e. Type A); (2) rollers move between a V-shaped sloping surface and a flat surface (i.e. Type B); (3) energy dissipation is only contributed by rolling friction; and (4) the adjustable linear spring modules embedded in the side plates can generate required normal forces to supply sliding friction forces between the side plates and bearing plates of the isolation device, as shown in Figure 1.

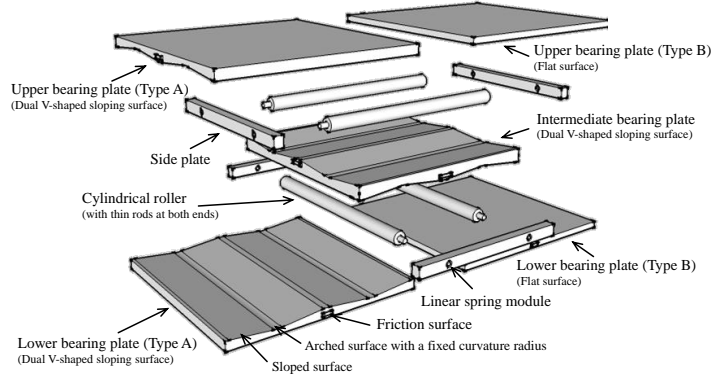


Figure 1. Schematic view of multi-roller bearing isolation devices

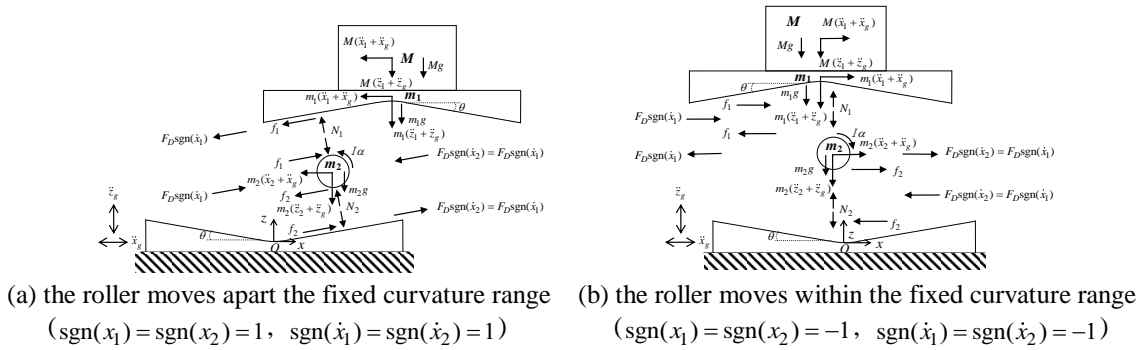


Figure 2. Free body diagram of Type A isolation device

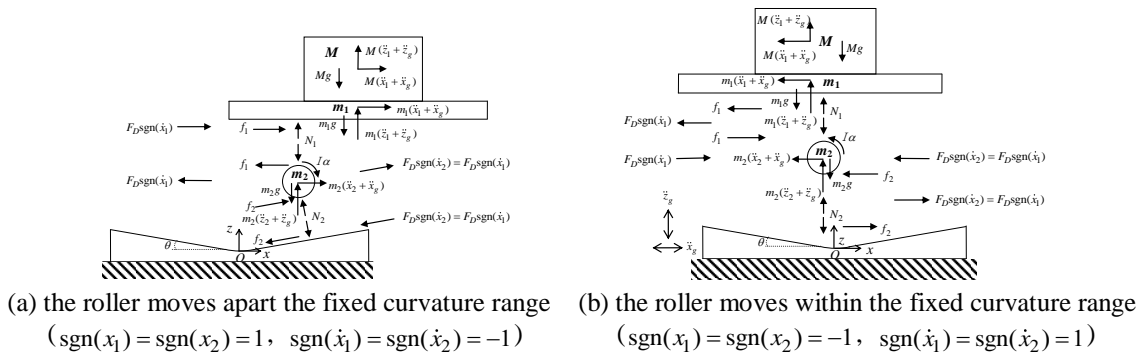


Figure 3. Free body diagram of Type B isolation device

The following basic assumptions are made first to facilitate the derivation of dynamic behavior of the multi-roller isolation device: (1) the rollers and bearing plates are ideally in pure rolling motion; (2) the motions of single roller between two opposite bearing plates (denoted as superior and inferior bearing plates hereafter) are derived, as shown in the simplified models of Figures 2 and 3; (3) the inferior bearing plate is fixed to be a rigid base; (4) the rolling friction force is considered in the derivation; (5) appropriate rigid-plastic hysteretic models are used to represent the force-displacement

relationships of rolling and sliding friction behavior; and (6) Two opposite rolling motion directions when the superior bearing plate (or the roller) is rightward and leftward relative to the inferior bearing plate are (totally four conditions) considered in the derivation.

The free body diagram of Type A isolation device when the roller moves apart from the fixed curvature range is shown in Figure 2(a), in which \ddot{x}_g and \ddot{z}_g = the horizontal and vertical acceleration excitations; θ is the sloping angle of the V-shaped surfaces; M , m_1 and m_2 = the seismic reactive masses of the protected object, superior bearing plate and roller, respectively; I = moment of inertia of the roller; g = the acceleration of gravity; α = the angular acceleration of the roller; $x_1(z_1)$, $\dot{x}_1(\dot{z}_1)$ and $\ddot{x}_1(\ddot{z}_1)$ = the horizontal (vertical) displacement, velocity and acceleration responses of the protected object and superior bearing plate relative to the origin O , respectively; $x_2(z_2)$, $\dot{x}_2(\dot{z}_2)$ and $\ddot{x}_2(\ddot{z}_2)$ = the horizontal (vertical) displacement, velocity and acceleration responses of the roller relative to the origin O , respectively; f_1 and f_2 = the nominal rolling forces acting between the superior bearing plate and roller and between the roller and inferior bearing plate, respectively; N_1 and N_2 = the normal forces acting between the superior bearing plate and roller and between the roller and inferior bearing plate, respectively; $F_{r1} = \mu_r N_1$ and $F_{r2} = \mu_r N_2$ = the predicted rolling friction forces acting between the superior bearing plate and roller and between the roller and inferior bearing plate, respectively, in which μ_r = the ratio of the rolling resistant coefficient (δ) to the roller radius (r) (Shames, 1996); and F_D = the sliding friction force acting parallel to the slope of the bearing plates contributed by the supplemental energy dissipation devices. Taking the dynamic force equilibrium of $M + m_1$ and m_2 along x and z directions together with the dynamic moment equilibrium of m_2 , neglecting $m_2 / (M + m_1)$ due to the fact that m_2 is in general much less than $M + m_1$, one can solve \ddot{x}_1 and \ddot{z}_1 , find that N_1 is very close to N_2 , and obtain that f_1 and f_2 mathematically approach to null values and can be rationally replaced by $F_{r1} = F_{r2} = \mu_r N$, as given in Equations (2.1.1) to (2.1.3).

$$\ddot{x}_1 = -\ddot{x}_g \cos^2 \theta - \frac{1}{2}(g + \ddot{z}_g) \sin 2\theta \operatorname{sgn}(x_1) - \frac{(\mu_r N + F_D)}{(M + m_1)} \cos \theta \operatorname{sgn}(\dot{x}_1) \quad (2.1.1)$$

$$\ddot{z}_1 = -(\ddot{z}_g + g) \sin^2 \theta - \frac{1}{2} \ddot{x}_g \sin 2\theta \operatorname{sgn}(x_1) - \frac{(\mu_r N + F_D)}{(M + m_1)} \sin \theta \operatorname{sgn}(\dot{x}_1) \quad (2.1.2)$$

$$N (\approx N_1 \approx N_2) = (M + m_1) \left[g \cos \theta + \ddot{z}_g \cos \theta - \ddot{x}_g \sin \theta \operatorname{sgn}(x_1) \right] \quad (2.1.3)$$

Assuming θ is tiny such that $\cos^2 \theta \approx 1$ and $\sin^2 \theta \approx 0$, the transmitted acceleration response for Type A isolation device along the horizontal direction when the roller moves apart from the fixed curvature range are obtained as

$$\ddot{x}_1 + \ddot{x}_g = -\frac{1}{2}(g + \ddot{z}_g) \sin 2\theta \operatorname{sgn}(x_1) - \frac{(\mu_r N + F_D)}{(M + m_1)} \cos \theta \operatorname{sgn}(\dot{x}_1) \quad (2.1.4)$$

and those along the vertical direction when the roller moves apart from the fixed curvature range are obtained as

$$\ddot{z}_1 + \ddot{z}_g = \ddot{z}_g - \frac{1}{2} \ddot{x}_g \sin 2\theta \operatorname{sgn}(x_1) - \frac{(\mu_r N + F_D)}{(M + m_1)} \sin \theta \operatorname{sgn}(\dot{x}_1) \quad (2.1.5)$$

When the roller moves within the fixed curvature range, as shown in Figure 2(b), the sloping angle of the round surface is no longer a constant value and is much less than that of the inclined surface.

Assuming $\cos\theta \approx 1$ and $\sin\theta \approx x_1/2R$ in which R is the fixed curvature radius in the range between two inclines of the V-shaped surface of the bearing plate, the transmitted acceleration responses for Type A isolation device along the horizontal and vertical directions when the roller moves within the fixed curvature range can be expressed in a simplified form

$$\ddot{x}_1 + \ddot{x}_g = -\frac{(g + \ddot{z}_g)\text{sgn}(x_1)}{2R}x_1 - \frac{(\mu_r N + F_D)}{(M + m_1)}\text{sgn}(\dot{x}_1) \quad (2.1.6)$$

$$\ddot{z}_1 + \ddot{z}_g = \ddot{z}_g - \frac{1}{2R}\left[\ddot{x}_g\text{sgn}(x_1) + \frac{(\mu_r N + F_D)}{(M + m_1)}\right]x_1 \quad (2.1.7)$$

In addition, Figure 3(a) illustrates the free body diagram of Type B isolation device when the roller moves apart from the fixed curvature range. The notation definitions in Figures 2 and 3 are identical. In the same manner as the above derivation for Type A isolation device, and assuming $\theta/2$ is tiny such that $\cos^2(\theta/2) \approx 1$, $\sin^2(\theta/2) \approx 0$ and $\sin^2\theta \approx 0$, the transmitted acceleration responses for Type B isolation device along the horizontal and vertical directions when the roller moves apart from the fixed curvature range can be written as

$$\ddot{x}_1 + \ddot{x}_g = -\frac{1}{2}(g + \ddot{z}_g)\sin\theta\text{sgn}(x_1) - \frac{(\mu_r N + F_D)}{(M + m_1)}\text{sgn}(\dot{x}_1) \quad (2.1.8)$$

$$\ddot{z}_1 + \ddot{z}_g = \ddot{z}_g - \frac{1}{2}\ddot{x}_g\sin\theta\text{sgn}(x_1) - \frac{(\mu_r N + F_D)}{(M + m_1)}\tan\frac{\theta}{2}\text{sgn}(\dot{x}_1) \quad (2.1.9)$$

Similar to the above assumptions for Type A isolation device, the transmitted acceleration responses for Type B isolation device along the horizontal and vertical directions when the roller moves within the fixed curvature range, as shown in Figure 3(b), can be expressed in a simplified form

$$\ddot{x}_1 + \ddot{x}_g = -\frac{(g + \ddot{z}_g)\text{sgn}(x_1)}{4R}x_1 - \frac{(\mu_r N + F_D)}{(M + m_1)}\text{sgn}(\dot{x}_1) \quad (2.1.10)$$

$$\ddot{z}_1 + \ddot{z}_g = \ddot{z}_g - \frac{1}{4R}\ddot{x}_g\text{sgn}(x_1)x_1 \quad (2.1.11)$$

The compatibility conditions for Type A and Type B isolation devices are essentially different due to the fact that these two isolation devices have different superior bearing plate surfaces in contact with rollers. For Type A isolation device, the horizontal and vertical responses of the superior bearing plate are twice those of the roller. For Type B isolation device, the horizontal responses of the superior bearing plate are still twice those of the roller if $\cos\theta$ can be approximated to be 1, while the vertical responses of the superior bearing plate are the same as those of the roller. The discrepancy of dynamic responses between Type A and Type B isolation devices are further discussed as follows.

- (1) When the roller moves apart from the fixed curvature range and without considering \ddot{z}_g , $\mu_r N$ and F_D , the horizontal transmitted acceleration responses can behave as an ideally constant level which is simply bounded by θ . In addition, without considering $\mu_r N$ and F_D , the dynamic behavior of Type A isolation device with a sloping angle of θ should be mathematically identical to that of Type B isolation device with a sloping angle of 2θ .
- (2) When the roller moves within the fixed curvature range and without considering \ddot{z}_g , $\mu_r N$ and F_D , the horizontal transmitted acceleration responses are inversely proportional to R . In addition, without considering $\mu_r N$ and F_D , the dynamic behavior of Type A isolation device with a curvature radius of $2R$ should be mathematically identical to that of Type B isolation device with a

curvature radius of R .

- (3) All the equations excluding F_D can be used to represent the dynamic behavior of the isolation devices without supplement sliding friction capabilities.
- (4) The dynamic behavior of the conventional isolation devices when the roller passes through the valley of the V-shaped surface without a fixed curvature range can also be represented by the obtained equations in which R should be replaced by the roller radius r .

2.2. Simplified Hysteretic Model

The hysteretic behavior of the isolation devices with and without supplement sliding friction capabilities subjected to horizontal excitations can be simulated by a simplified twin-flag hysteretic model (Inaudi *et al.*, 1990) consisting of “MultiLinear Elastic” Model and “Plastic” Model (Wen, 1976) in the readily available analysis programs, as illustrated in Figure 4. When the roller moves within the fixed curvature range, the first slopes of “MultiLinear Elastic” Models for Type A and Type B isolation devices are respectively assigned to be $(M + m_1)g / 2R$ and $(M + m_1)g / 4R$ according to Equations (2.1.6) and (2.1.10). When the roller moves apart from the fixed curvature range, the second slopes of “MultiLinear Elastic” Models for Type A and Type B isolation devices are perfectly plastic with constant levels of $(M + m_1)g \sin 2\theta / 2$ and $(M + m_1)g \sin \theta / 2$, respectively, according to Equations (2.1.4) and (2.1.8). No matter when the roller moves within or apart from the fixed curvature range, the characteristic strengths of “Plastic (Wen)” models for Type A and Type B isolation devices are simplified to be equal to $\mu_r N + F_D$ (or $\mu_r N$ if supplement sliding friction is not provided) in which N can be further simplified to be $M + m_1$.

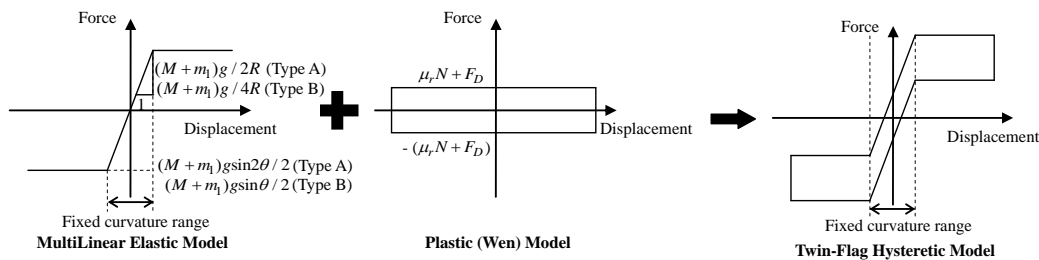


Figure 4. Simplified hysteretic models to represent dynamic behavior of multi-roller isolation devices

3. EXPERIMENTAL STUDY

3.1. Test Models

Three shaking table test schemes are conducted in this study. The upper, intermediate and lower bearing plates of the test multi-roller isolation devices have a plan dimension of 600mm by 600mm , and the cylindrical rollers have a sectional radius (r) of 17.5mm and a longitudinal length of 600mm . The allowable maximum displacement of the isolation devices is design to be 250mm . A range of 20.91mm ($\pm 10.455\text{mm}$) with a curvature radius (R) of 100mm is reserved between two inclines of the V-shaped surfaces of the bearing plates. In Test Scheme I, five multi-roller isolation devices including Type A and Type B isolation devices with different supplemental sliding friction capabilities, denoted as Bearings A-1, A-2, A-3, B-1 and B-2 and described in detail in Table 1. The protected equipment above the isolation devices is simulated by lead blocks with a total seismic reactive mass of $500\text{N} - \text{sec}^2 / m$, as shown in Figure 5. In Test Scheme II, the effectiveness of implementation of Type A isolation devices without supplement sliding friction capability into four plane arrangements of reservation cabinets (as illustrated in Figure 6) in seismic response reduction are discussed. The dimension of one set of reservation cabinet is about 1445mm (width in the longitudinal direction) \times

600mm (depth in the transverse direction) \times 1589mm (height). The seismic reactive mass of a set of vacant reservation cabinet is about $377.2 N - sec^2 / m$. It should be noted that in the fourth plane arrangement shown in Figure 6(d), the added linking beams across the tops of two assemblages of three sets of reservation cabinets that do not obstruct the usual working space can effectively improve the aspect and plane dimension ratios of integral of reservation cabinets and can essentially enhance the stability performance. The plane dimensions, aspect ratios and plane dimension ratios of all the plane arrangements are summarized in Table 2. In Test Scheme III, the effectiveness of incorporation of four Type B isolation devices with appropriate supplement sliding friction capability into a raised floor system (3m by 3m in plane dimension) in seismic response reduction is studied. The protected equipment above the isolated raised floor system is simulated by lead blocks with a total seismic reactive mass of $1000 N - sec^2 / m$, as shown in Figure 7.

Table 1. Design parameters of different multi-roller isolation devices in Test Scheme I

Bearing No.	Bearing Type	Design Parameters		
		Sloping angle of V-Shaped Surface		Normal Force for Sliding Friction Force Applied on Each Side Plate
		Upper and Lower Bearing Plate	Intermediate Bearing Plate	
A-1	A	6.25 degrees	6.25 degrees	w/o
A-2	A	6.25 degrees	6.25 degrees	332.52N
A-3	A	6.25 degrees	6.25 degrees	665.04N
B-1	B	flat	6.25 degrees	w/o
B-2	B	flat	6.25 degrees	332.52N

Table 2. Geometric properties of four plane arrangements of reservation cabinets in Test Scheme II

	Plane Dimension (mm)		Aspect Ratio		Plane Dimension Ratio
	X dir.	Y dir.	X dir.	Y dir.	
First Plane Arrangement	1445	600	1.10	2.65	2.41
Second Plane Arrangement	4335	600	0.37	2.65	7.23
Third Plane Arrangement	4335	1200	0.37	1.32	3.61
Fourth Plane Arrangement	4335	2500	0.37	0.64	1.73



(a) Type A isolation Bearings (A-1, A-2 and A-3)

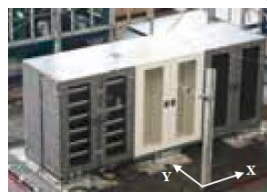


(b) Type B isolation Bearings (B-1 and B-2)

Figure 5. Installation of test models in Test Scheme I



(a) first arrangement (without and with isolation devices)



(c) third arrangement



(b) second arrangement



(d) fourth arrangement

Figure 6. Installation of reservation cabinets with four plane arrangements in Test Scheme II



Figure 7. Installation of the isolated raised floor system in Test Scheme III

3.2. Test Program

In addition to two artificial acceleration histories compatible with the required response spectra that are determined in accordance with AC156 (denoted as AC156-TAP090 and AC156-TCU054 hereafter), two ground motions recorded at I-ELC270 and KJM000 stations respectively during the 1940 El Centro earthquake and 1995 Kobe earthquake (denoted as I-ELC270 and KJM000 hereafter)

are considered for all the shaking table test schemes, as summarized in Table 3. All the shaking table test schemes are subjected to uniaxial horizontal acceleration excitations in the X and Y directions.

Table 3. Acceleration excitation program

Test Name		Input Earthquake Information or Response Spectra Condition	Targeted Input Peak Acceleration (g)
Artificial Acceleration History	AC156- TAP090	Near TAP090 station, reinforced concrete structures (7 stories, 24m in height), isolated equipment is placed at 3rd floor (8.75m in elevation)	0.50
	AC156- TCU054	Near TAP054 station, reinforced concrete structures (3 stories, 12m in height), isolated equipment is placed at 3rd floor (8m in elevation)	1.00
Recorded Earthquake History	I-ELC270	El Centro/I-ELC270, Imperial Valley, U.S., 1940/05/19	0.36
	KJM000	KJMA/KJM000, Kobe, Japan, 1995/01/16	0.78

3.3. Seismic Response

In Test Scheme I, the comparisons of hysteresis loops and horizontal seismic response histories of different isolation bearings subjected to I-ELC270 in the X direction are illustrated in Figures 8 and 9, respectively. It is of no surprise that the increase in supplemental sliding friction will lead to the reduction of peak displacement responses and the augment of peak transmitted acceleration responses, and the oscillation after input excitations will also be damped more effectively. Furthermore, as indicated in the above analytical discussion, it is reasonable that the peak transmitted acceleration response of Type B isolation device is smaller than that of Type A isolation device while subjected to the same input excitation. Assuming the rolling friction contribution is very limited in Bearings A-1 and B-1, it can be found that the peak transmitted acceleration ratio of Bearings A-1 to B-1 is very close to $\sin(2\theta)/\sin(\theta) \approx 2$. More importantly, the test results show that under the same input excitation, the peak displacement response of Type B isolation device is usually less than that of Type A isolation device, which can be clarified using the definition of equivalent damping ratios. In Test Scheme II, the horizontal seismic response histories at the top of reservation cabinets with different plane arrangements under AC156-TAP090 and AC156-TCU054 in the X direction are depicted in Figure 10. Since the plane dimension ratio of the assemblage of three sets of reservation cabinets is the largest (or most irregular) among all the plane arrangements, as summarized in Table 2, the effect arose from irregularity may not be negligible. Even so, the peak transmitted acceleration responses for all the plane arrangements are well controlled to be an ideally constant level as the design value, i.e. 0.12g. The comparisons of horizontal deflection responses of isolated reservation cabinets with four plane arrangements under AC156-TAP090 in the Y direction are illustrated in Figure 11. Although all the plane arrangements equipped with the isolation devices have a satisfactory performance in relieving horizontal deflection responses of reservation cabinets, the assemblages of reservation cabinets have a better performance than one set of reservation cabinet, especially for the fourth plane arrangement. The comparison of rotation extents of isolated reservation cabinets with the third and fourth plane arrangements subjected to AC156-TAP090 in the Y direction are illustrated in Figure 12. Due to a larger plane dimension of the integral of reservation cabinets, the fourth plane arrangement has a better plane rotation resistant capability than the third plane arrangement. In Test Scheme III, the horizontal transmitted acceleration response history and hysteresis loops of the isolated raised floor system under AC156-TCU054 in the X direction are depicted in Figure 13. The peak transmitted acceleration response can be drastically reduced in comparison with the input peak acceleration value and can still reveal a desired steady level. Since the supplemental sliding friction is engaged, the hysteresis loops reveal a good energy dissipation capability.

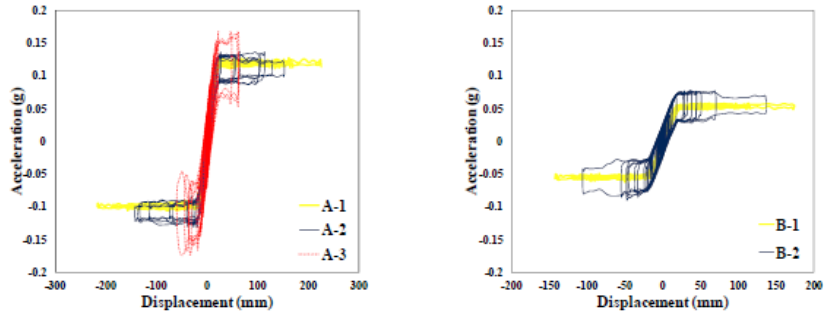


Figure 8. Hysteretic loops of different isolation bearings under I-ELC270

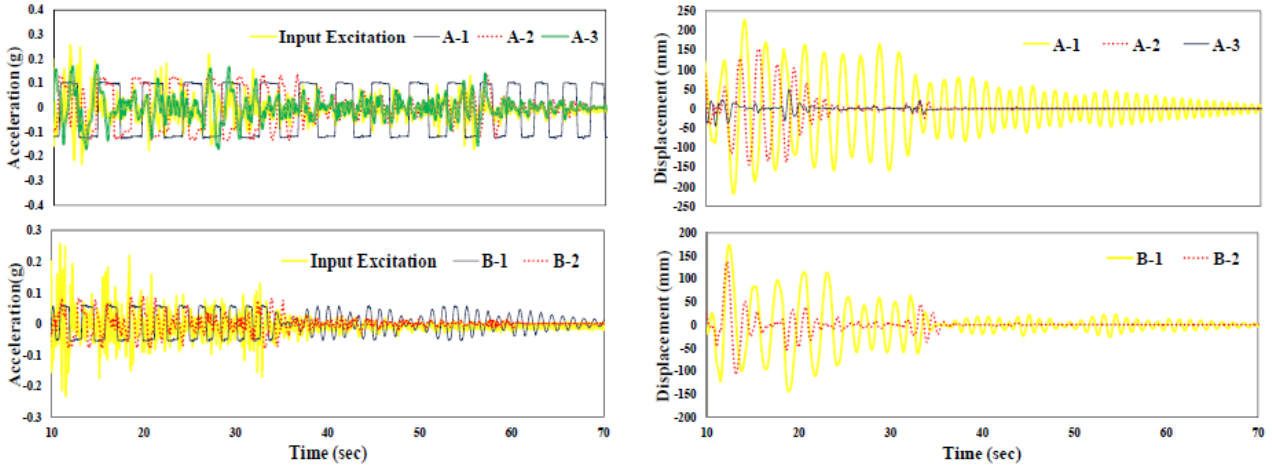
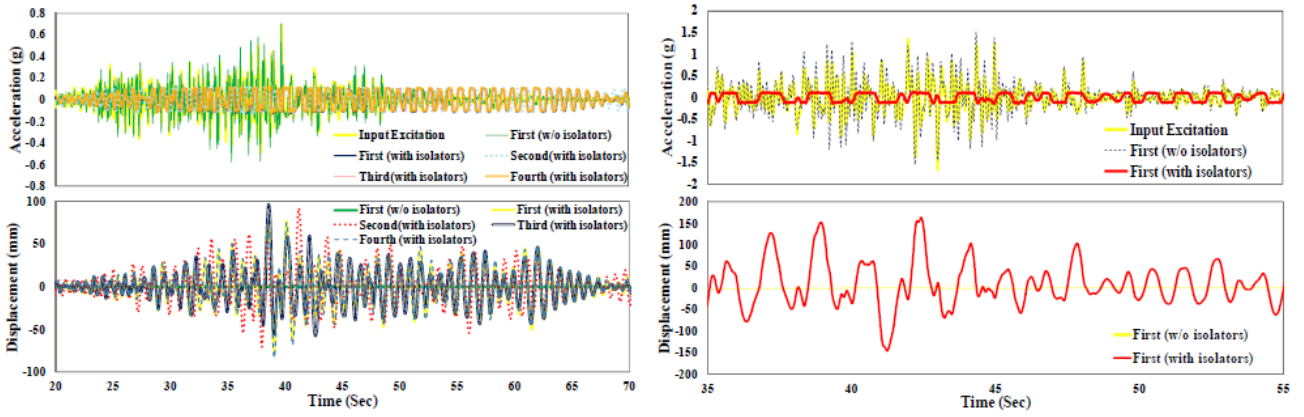


Figure 9. Seismic response histories of different isolation bearings under I-ELC270



(a) under AC156- TAP090

(b) under AC156- TCU054

Figure 10. Seismic response histories of reservation cabinets with different plane arrangements

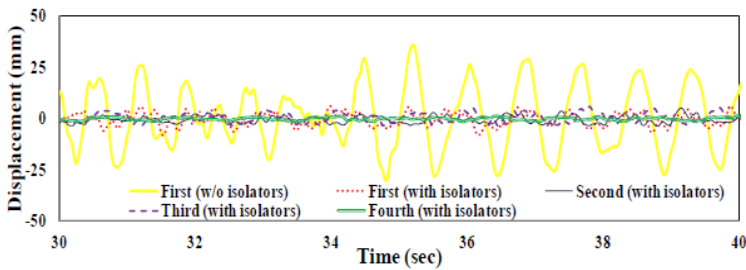


Figure 11. Horizontal deflection responses of isolated reservation cabinets with different plane arrangements under AC156-TAP090

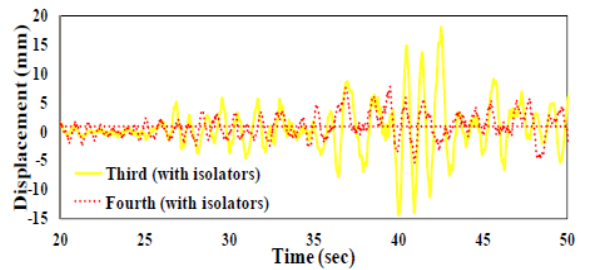


Figure 12. Plane rotation extents of isolated reservation cabinets with different plane arrangements under AC156-TAP090

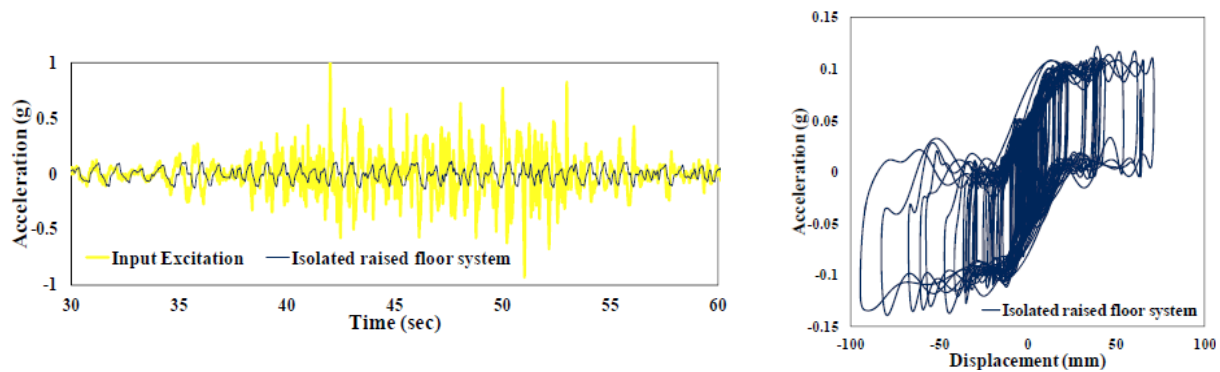


Figure 13. Acceleration response histories and hysteresis loops of isolated raised floor system under AC156-TCU054

4. CONCLUSIONS

Among currently well-developed seismic isolation devices, the sloped rolling-type isolation device can offer maximum horizontal decoupling between the protected object and input excitations, which may most easily meet the rigorous performance-based design requirements. The sloped rolling-type isolation device equipped with two pairs of mutually orthogonal rollers, i.e. the multi-roller isolation device, is focused in this study. Based on the analytical results, the design requirements are further discussed, and a simplified twin-flag hysteretic model is proposed to appropriately represent the hysteretic behavior of the isolation device. Several plane arrangements of isolated reservation cabinets and an isolated raised floor system subjected to recorded strong ground motions and artificial acceleration histories are performed in the shaking table test schemes. The experimental results show the high efficiency of using the multi-roller isolation device in seismic protection of reservation cabinets and important equipment above an isolated raised floor system.

REFERENCES

- Hamidi M, ElNaggar MH, Vafai A, Ahmadi G. (2003). Seismic isolation of buildings with sliding concave foundation (SCF), *Earthquake Engineering and Structural Dynamics* **32**, 15-29.
- Hwang JS, Huang YN, Hung YH, Huang JC. (2004). Applicability of seismic protective systems to structures with vibration sensitive equipment. *Journal of Structural Engineering ASCE* **130:11**, 1676-1684.
- Inaudi JA, Kelly JM. (1990). Active isolation. *Proceeding of the U.S. National Workshop on Structural Control Research*, October.
- Lee GC, Ou YC, Niu T, Song J, Liang Z. (2010). Characterization of a roller seismic isolation bearing with supplemental energy dissipation for highway bridges. *Journal of Structural Engineering, ASCE* **136:5**, 502-510.
- Lin TW, Hone CC. (1993). Base isolation by free rolling rods under basement. *Earthquake Engineering and Structural Dynamics* **22**, 261-73.
- Lu LY, Lin GL. (2008). Predictive control of smart isolation system for precision equipment subjected to near-fault earthquakes. *Engineering Structures* **30**, 3045-3064.
- Myslimaj B, Gamble S, Chin-Quee D, Davies A. (2003). Base isolation technologies for seismic protection of museum artifacts. *The 2003 IAMFA Annual Conference*, San Francisco, California, September 21-24.
- Naeim F, Kelly JM. (1999). Design of seismic isolated structures: from theory to practice. *Wiley, New York*.
- Shames IH. (1996). Engineering Mechanics: Dynamics. *Eaglewood Cliffs (NJ): Prentice-Hall Inc.* **4th Ed.**
- Tsai MH, Wu SY, Chang KC, Lee GC. (2007). Shaking table tests of a scaled bridge model with rolling type seismic isolation bearings. *Engineering Structures* **29:9**, 694-702.
- Wen YK. (1976). Method for random vibration of hysteretic systems. *Journal of Engineering Mechanics, ASCE* **102:2**, 249-263.
- Zhou Q, Lu X, Wang Q, Feng D, Yao Q. (1998). Dynamic analysis on structures base-isolated by a ball system with restoring property. *Earthquake Engineering and Structural Dynamics* **27**, 773-791.
- (2007). Acceptance Criteria for Seismic Qualification by Shake-table Testing of Nonstructural Components and Systems. *ICC Evaluation Service inc.* **AC156**.